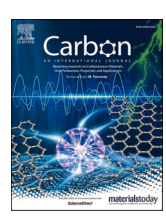
ELSEVIER

Contents lists available at ScienceDirect

Carbon

journal homepage: www.elsevier.com/locate/carbon





Resonance Raman spectroscopy characterization of linear carbon chains encapsulated by multi-walled carbon nanotubes

Thiago A. Moura ^{a,b}, Wellington Q. Neves ^b, Rafael S. Alencar ^c, Y.A. Kim ^d, M. Endo ^e, Thiago L. Vasconcelos ^f, Deyse G. Costa ^g, Graziâni Candiotto ^h, Rodrigo B. Capaz ^{h,i}, Paulo T. Araujo ^{j,**}, Antonio G. Souza Filho ^a, Alexandre R. Paschoal ^{a,j,*}

- ^a Departamento de Física, Universidade Federal do Ceará, Fortaleza, Ceará, 60455-900, Brazil
- ^b Instituto Federal de Educação, Ciência e Tecnologia do Ceará, Fortaleza, Ceará, 60040-531, Brazil
- ^c Faculdade de Física, Universidade Federal do Pará, Belém, Pará, 66075-110, Brazil
- ^d Department of Polymer Engineering, Graduate School, School of Polymer Science and Engineering & Alan G. MacDiarmid Energy Research Institute, Chonnam National University, 77 Yongbong-ro, Buk-gu, Gwangju, 61186, South Korea
- ^e Faculty of Engineering, Shinshu University, 4-17-1 Wakasato, Nagano-shi, 380-8553, Japan
- f Divisão de Metrologia de Materiais, Instituto Nacional de Metrologia, Qualidade e Tecnologia (INMETRO), Duque de Caxias, Rio de Janeiro, 25250-020, Brazil
- g Departamento de Química, Universidade Federal de Viçosa, Viçosa, MG, 36570-900, Brazil
- ^h Instituto de Física, Universidade Federal Do Rio de Janeiro, Rio de Janeiro, RJ, 21941-972, Brazil
- i Brazilian Nanotechnology National Laboratory (LNNano), Brazilian Center for Research in Energy and Materials (CNPEM), Campinas, SP, 13083-100, Brazil
- ^j Department of Physics and Astronomy, University of Alabama, Tuscaloosa, AL, 35487, USA

ARTICLE INFO

Keywords: Linear carbon chains Carbon nanotubes Raman spectroscopy TERS

ABSTRACT

The unique electronic and vibrational properties of linear carbon chains (LCCs) have attracted close attention from the scientific community in recent years. Raman spectroscopy addressing the LCC spectral signature around 1850 cm⁻¹ has been widely used to identify the LCC and probe electronic and vibrational properties as a function of carbon length. Despite the number of works available in literature, some aspects of the LCC's aforementioned properties remain unclear. Using a combination of confocal and Tip-enhanced Raman Spectroscopy (TERS), along with different laser lines, this work addresses important aspects of the optical resonance window of LCCs encapsulated by multi-walled carbon nanotubes (MWCNTs) (i.e. LCC@MWCNT) as well as an elusive Raman signature around 1637 cm⁻¹, which is assigned to the LCC's longitudinal acoustic (LA) phonon mode at the X point (zone edge), which becomes Raman active likely due to disorder effects. First-principles calculations endorse our conclusions.

1. Introduction

Linear carbon chains (LCC) were theoretically proposed in the 1960s as an allotropic form of carbon presenting *sp* hybridization. There are two classifications for such LCCs: (1) polyynes, which are statistically more stable and display alternating triple and single bonds between constituent carbon atoms; and (2) cumulenes, which display only double bonds between constituent carbon atoms. The stability of these chains was, however, questioned until 2010, when a linear chain of 44 carbon atoms was successfully synthesized and stabilized by tris(3,5-dit-butylphenyl)methyl terminal groups [1]. The challenges in the synthesis of carbynes are mostly associated with their high instability and

reactivity with their environment [2,3]. These drawbacks have been circumvented by techniques that facilitate the synthesis of LCCs confined in the hollow cavities of carbon nanotubes [4–6]. These techniques led to the synthesis of longer length carbynes (containing more than 6000 carbon atoms) [7] and they remain cohesive even at high temperatures and pressures [8].

The potential applications and outstanding properties of LCCs have boosted their scientific appeal, which follows the path of other allotropic forms of carbon such as carbon nanotubes [9], fullerenes [10] and graphene [11]. LCCs are predicted to be more resistant than any other material [12]; to have unique conductive properties [13]; and to possess a size-dependent band gap, which place them ahead in the development

E-mail addresses: paulo.t.araujo@ua.edu (P.T. Araujo), paschoal@fisica.ufc.br (A.R. Paschoal).

^{*} Corresponding author. Departamento de Física, Universidade Federal Do Ceará, Fortaleza, Ceará, 60455-900, Brazil.

^{**} Corresponding author.

of novel electronic nanodevices. These LCCs also possess a number of unique responses to external stimuli (e.g. pressure and temperature) and a summary of the mechanical properties predicted for LCC can be found in Ref. [14] and in Refs. [15,16].

Raman Spectroscopy is a key technique for studying the physical and chemical properties of carbon nanomaterials [17–19]. The Raman spectrum of LCCs carries a size-dependent signature (from now on Cn peak) whose frequency spans around 1850 cm⁻¹ at ambient conditions [20]. According to Tip-enhanced Raman experiments by Tschannen *et* al., LCCs possess the highest resonance differential Raman cross section per atom ever reported [21]. This Cn peak is also an excellent probe for investigating LCCs' thermal and mechanical properties. Costa et al. used the Cn peak frequency as a probe to access the heat capacities and thermal coefficient expansions of LCCs by carrying out low temperature measurements [22]. The mechanical properties of LCCs were studied by Sharma et al., where the authors observed that the Young modulus and Grüneisen parameter obey a P⁻¹ power law dependence with pressure [23].

Despite the recent advances in understanding the science of LCCs, there is still a great deal of work to be done on the vibrational and electronic properties of these materials when they are interacting with an external environment (e.g. LCCs encapsulated by carbon nanotubes). In this work, we studied the LCC's electronic and vibrational properties using confocal and tip-enhanced Raman spectroscopy (TERS) in individual LCC@MWCNT systems or very small bundles. Using these techniques along with a set of different laser lines, the optical resonance window of LCCs encapsulated by MWCNTs (from now one LCC@MWCNTs) is addressed, and a thus far elusive Raman signature around 1637 cm⁻¹, which is assigned to the LCC's longitudinal acoustic LA(X) phonon mode at the Brillouin Zone edge, is also reported.

2. Experimental

2.1. Sample preparation

Linear carbon chains encapsulated by multiwalled carbon nanotubes (LCC@MWCNT) studied in this work were synthetized by the controlled arch discharge method [24] and have already been characterized by electron microscopy [25] and investigated under high pressure Raman Spectroscopy [15,26,27]. Aiming to characterize isolated tube of LCC@MWCNTs, the bulk sample was subjected to standard bath sonication and centrifugation process using acetone as a dispersive medium followed by deposition on a glass coverslip in order to obtain a good concentration of dispersed LCC@MWCNT. The choice for acetone as dispersive medium resides on its fast evaporation when drop-casted over the coverslip leaving only the dispersed LCC@MWCNT with minimum amount of residues when compared to other dispersion media such as DNA or SDS. Atomic Force Microscopy (AFM) was then employed to verify if isolated nanotubes were obtained after the dispersion process.

2.2. Techniques

Individual LCC@MWCNT, previously characterized via AFM, were initially analyzed by confocal Raman Spectroscopy using laser excitations of $E_L=1.96~\rm eV$ (632.8 nm) and $E_L=2.33~\rm eV$ (532 nm). To each excitation source, several spectra of individualized LCC@MWCNT were collected. The Confocal Raman spectra were acquired using an Alpha 300 system from Witec (Ulm, Germany) equipped with a highly linear (0.02%) piezo-driven stage, a $100x/\rm NA=0.90~\rm Nikon$ objective, and with laser excitation HeNe (632.8 nm), argon (488 nm) and Nd:YAG (532 nm). The Raman signal was detected by a high-sensitivity, back illuminated CCD located behind a 600 l/mm grating. The spectrometer used was an ultra-high throughput Witec UHS 300 with up to 70% throughput, explicitly designed for Raman spectroscopy. Full width at half-maximum (FHWH) of the peak related to the Cn vibration, which is expected around $10~\rm cm^{-1}$, was used to distinguish the spectra of a single

or multiple LCCs encapsulated by the isolated MWCNTs.

In order to localize the interest sample positions on the coverslip surface, Raman mapping was performed by using the 488 nm excitation wavelenght (each spectra was recorded in a Witec Alpha 300 R spectrometer using a 100x amplification objective and a 600 grooves/mm gratting and an integration time of 1 s at each point) and confocal photomultiplier mapping associated with a bandpass filter was performed by means the 632.8 nm excitation wavelength (the setup assembled to the TERS measurements, a Shamroch SR303i spectrometer operating with a 600 grooves/mm grating and coupled to a iDUS CCD camera and a Excelitas cascade photomultiplier counter was also used to analyze the far field signal coming from the sample and collected by a 60x amplification immersion-oil objective). Altogether, the spectral resolution obtained is as high as $\pm~2~{\rm cm}^{-1}$. The Raman mapping was performed over a 10 μ m $\times~10~\mu$ m region, covered by a 64 x 64 grid, with an integration time of 10 s at each pixel.

For the TERS system setup, a radially polarized laser beam (632.8 nm, 1.96 eV) was focused on the sample from below using an inverted optical microscope (Nikon Eclipse Ti–U) and a homemade shear-force-based AFM system employing a plasmon-tunable gold tip pyramid [28]. To locate the sample of interest and guide the alignment of the tip with the laser beam, a photon counter was used, associated with a bandpass filter suitable for measuring the bands of the LCCs. The first TERS image, shown in Fig. 3, is a 640 nm \times 640 nm square, covered by a grid of 64 x 64 pixels, with an integration time of 0.4 s at each pixel for selected bands. The second TERS image (Fig. 4) was performed over a 320 nm \times 320 nm area covered by a grid of 32 x 32 pixels with an accumulation time of 1 s at each point.

3. Results

3.1. Confocal Raman characterization

In order to obtain an overview of our samples, Raman spectra of LCC@MWCNTs in bundles as well as of individual LCC@MWCNT systems excited at both 632.8 nm (1.96 eV) and 532.0 nm (2.33 eV) are shown in Fig. 1a and b, respectively. It is seen that the Cn peak frequencies are in the range from 1800 cm⁻¹ to 1850 cm⁻¹, indicating that LCCs with distinct lengths (i.e. distinct number of carbon atoms) are observed. The LCCs encapsulated by MWCNTs may interact with the tubes' innermost walls through van der Waals forces or charge transfer [29], but the pristine values of the Cn frequencies and linewidths measured here suggest such interactions are not taking place.

The topmost spectra in Fig. 1a (solid red curve using 632.8 nm) and 1b (solid green curve using 533.0 nm) were acquired from bundled asgrown LCC@MWCNT, while the series of spectra below each of them were acquired from isolated LCC@MWCNT systems after solution dispersion over a glass coverslip. In the spectra obtained from isolated LCC@MWCNTs, each Cn peak associated with distinct encapsulated LCCs were fitted using Lorentzian curves and the peak-center of each Lorentzian is represented by the grayish circles underneath the spectra from the as-grown LCC@MWCNT. As expected, the Raman spectra of the as-grown system is the result of a convolution of the individual contributions from each individual LCC in an isolated LCC@MWCNT. The spectra acquired with the different laser lines reveal a larger distribution of LCCs in resonance with the 632.8 nm laser in comparison with the distribution observed with the 532.0 nm laser line. The resonance depends on the structural and electronic properties of the LCC, and the results suggest that longer LCCs are readily accessed with lower laser energies, while shorter LCCs are readily accessed with higher laser energies. As expected, the result also suggests that the longer (shorter) the LCC the smaller (larger) its bandgap. Although the LCCs reported here are encapsulated by MWCNTs, our observations of the Cn peak and its dependence with distinct laser energies, its linewidth, as well as correlations between LCC's length and bandgap are in good agreement with recent studies on LCCs encapsulated by double-walled carbon nanotubes

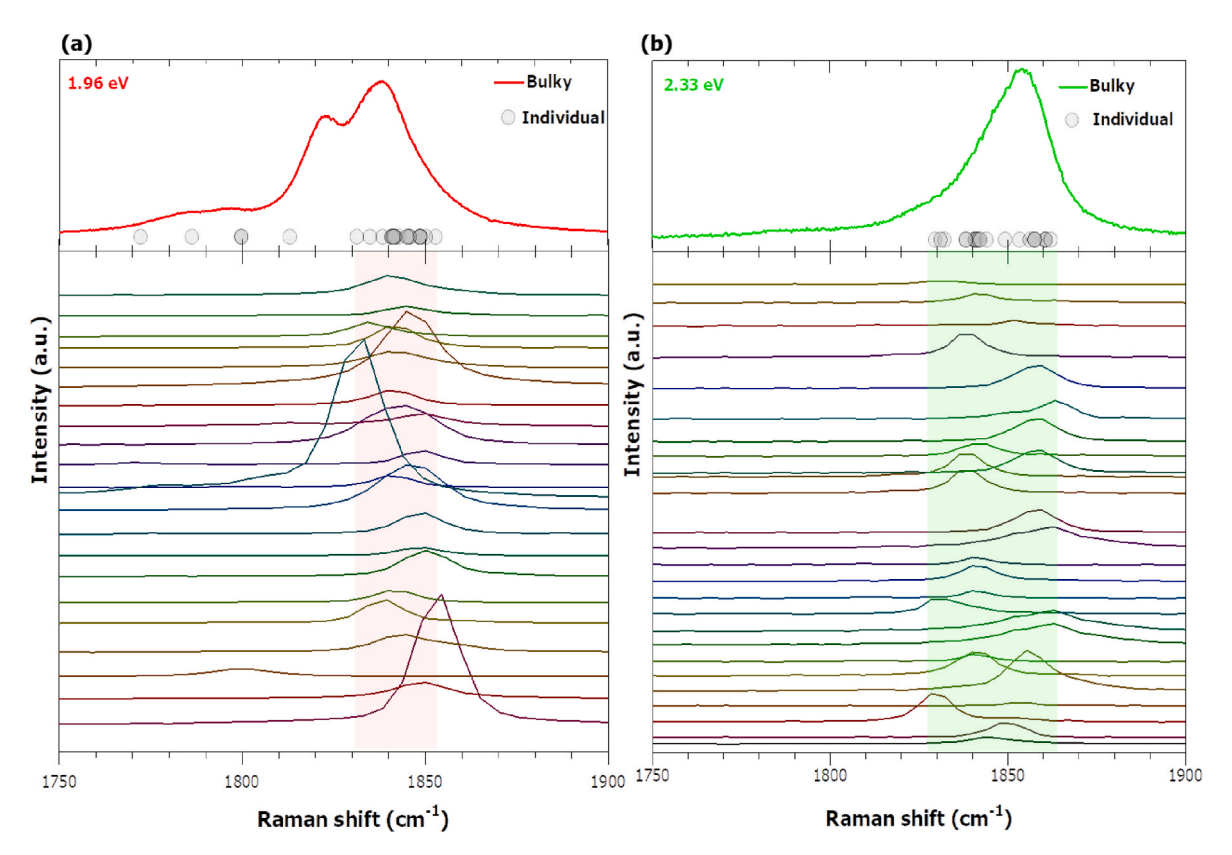


Fig. 1. Raman spectra collection of individual LCC@MWCNT excited at 632.5 nm (1.96 eV) (a) and 533.0 eV (2.33 eV) (b). For reference, the red-solid and the green-solid curves in (a) and (b) are the spectra of the bundled as-grown LCC@MWCNT that originated the individual LCC@MWCNTs after solution dispersion over a glass coverslip. In (a), each Raman spectrum representing individual LCC@MWCNT systems was fitted using Lorentzian curves and the Raman resonance frequency for each chain is represented by the greyish circles under the Raman spectra obtained from the as-grown systems. *The spectral resolution is* $\pm 2 \text{ cm}^{-1}$.

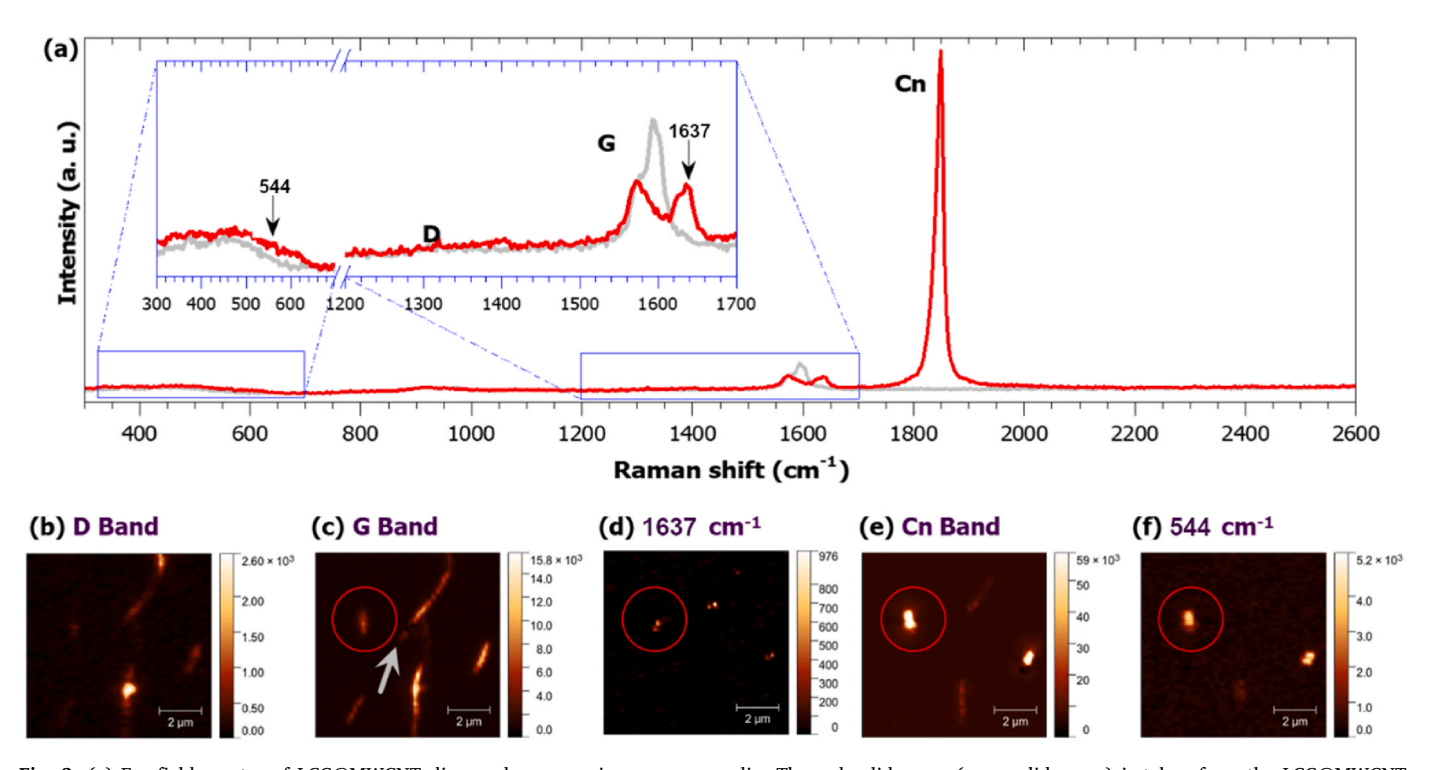


Fig. 2. (a) Far field spectra of LCC@MWCNT dispersed over a microscope coverslip. The red solid curve (gray solid curve) is taken from the LCC@MWCNT highlighted in (c) by the red circle (gray arrow). The images in (b) and (c) show, respectively, spectroscopic maps for the D- and G-bands associated with the dispersed nanotubes. (d), (e) and (f) show spectroscopic Raman images associated, respectively, with the elusive 1637 cm $^{-1}$ mode, the LCC Cn mode, and the mode around 544 cm $^{-1}$. The scale bar in the figure stands for 2 μ m length. The spectral resolution is \pm 2 cm $^{-1}$.

by Martinati et al. [30].

Fig. 2b-f shows Raman spectroscopic images of LCC@MWCNT systems dispersed in solution and then dropcasted on a glass coverslip. As indicated, the spatial mappings seen in Fig. 2b-f shows the intensities of several different Raman modes associated either with the hosting tubes (D- and G-bands) or with the LCCs (e.g. peak at 1637 cm⁻¹, Cn-band). The red (gray) spectrum shown in Fig. 2a was measured in the center of the circular region (tip of the arrow) indicated in Fig. 2c. Both spectra in Fig. 2a as well as the spectral maps in Fig. 2b and c shows that, although present in every MWCNT, the intensity of the D-band is very weak compared with the G-band. This suggests that effects associated with CNT disorder or adjacent walls interactions should be minimum [31]. As shown in Fig. 2e, the Cn Raman peak (Fig. 2e), is not present in every MWCNT. In fact, when compared to the maps in Fig. 2b and c, the map in Fig. 2e shows only three spots showing the Cn peak, which demonstrates that: (1) that the LCC is not present in every measured MWCNT; and (2) in most cases, the LCCs do not fill the entire CNT length. In addition, the map in Fig. 2d shows a novel Raman signature around 1637 cm⁻¹ on the right of the G-band (see inset in Fig. 2a). The inset in Fig. 2a and the map in Fig. 2f also show a spectral feature around 544 cm^{-1} [32], which will be discussed below.

3.2. Tip-enhanced Raman spectroscopy

In order to unveil the possible correlations among the spectral maps in Fig. 2d–f, the isolated LCC@MWCNT system highlighted by the red circle in Fig. 2c was further investigated via TERS, which provides detailed information about the encapsulated LCCs with high spatial resolution (typically below 50 nm) [33]. Fig. 3a shows a typical TERS spectrum of such isolated LCC@MWCNT system (see topographic image in the inset) displaying clear spectral signatures associated with the LCC Cn signature at 1846 cm⁻¹, with the hosting MWCNT at 1602 cm⁻¹ (G-band) and with the MWCNT disorder-induced band (D-band) at

 1350 cm^{-1} .

Fig. 3b shows the TERS image associated to the LCC $TO(\Gamma)$ mode around 544 cm⁻¹ [32]. Fig. 3c and d shows, respectively, spectroscopic maps of the quasi-negligible D- and the G-band of the host MWCNT. Fig. 3e and f show, respectively, the near-field spectroscopic map of the 1637 cm⁻¹ peak and of the LCC Cn mode around 1846 cm⁻¹. Note that the LCC in question is constituted of approximately 3800 carbon atoms. The calculation is made by considering the total length of the chain (~520 nm as suggested by the map in Fig. 3f) divided by 2.7 Å, which is an average of the lengths associated to single and triple bonds in the unit cell of the carbon chain, as pointed out by Ref. [34], then multiplied by 2, the number of carbon atoms in the unit cell. It is worth mentioning that a given MWCNT can have either one or multiple distinct LCCs encapsulated by it, and according to the literature [20], the Cn Raman peak for a single LCC encapsulated by a MWCNT is expected to be symmetric with a full-width at half maximum (FWHM) around 10 cm⁻¹. The FWHM of the Cn peak in Fig. 3a is \sim 14.2 cm⁻¹, which suggests that the isolated LCC@MWCNT in Fig. 3 is likely encapsulating two distinct LCCs with very close Cn frequencies; close enough not to be resolved within our equipment resolution of ± 2 cm⁻¹.

It is noticeable that, although the novel signature around $1637~{\rm cm}^{-1}$ (inset of Fig. 3a) is present in the near-field measurements, it is not manifested throughout the full length of the hosting MWNCT (see Fig. 3d). This pattern is also observed for the signature around $544~{\rm cm}^{-1}$ (see Fig. 3b), which reinforces the hypothesis that these two modes are LCC modes. In particular, the mode around $544~{\rm cm}^{-1}$ is understood to come from a LCC transverse optical mode at the Γ -point TO (Γ), as explained further in the text (and endorsed by our theoretical calculations). It is important to point that our assignment is in agreement with reports by Casari et al. [35]. We note that low frequency modes around 550 cm-1 have been observed for other carbon materials: Liu et al. observed traverse acoustic (TA) modes with such a frequency in graphyne nanotubes [36], while Jinno et al. observed such low

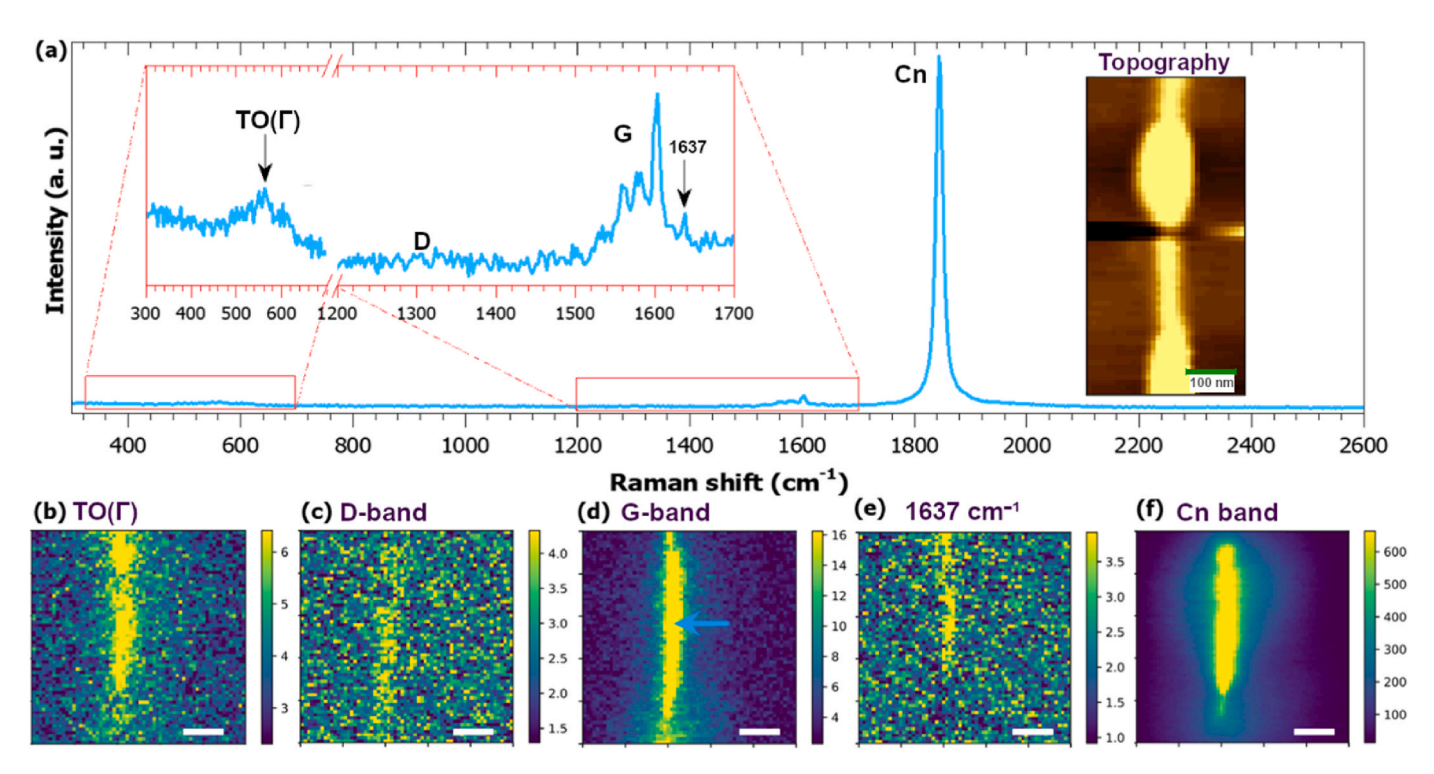


Fig. 3. (a) TERS spectra obtained from the LCC@MWCNT system in the point indicated by the blue arrow in (d). The topography AFM image is show in the inset of the figure; the widened regions correspond to places where some solvent-related residues remained after solution dispersion over the glass coverslip. (b) Spectral image associated to the LCC $TO(\Gamma)$ mode; (c) D-band spectral image associated with the hosting MWCNT; (d) TERS image map from the hosting MWCNT G band; (e) and (f) show the TERS image map associated with the frequencies of 1637 cm⁻¹ (assigned to the LA(X) mode) and 1846 cm⁻¹ (LCC Cn mode). The white scale bar is 130 nm. The spectral resolution is ± 2 cm⁻¹.

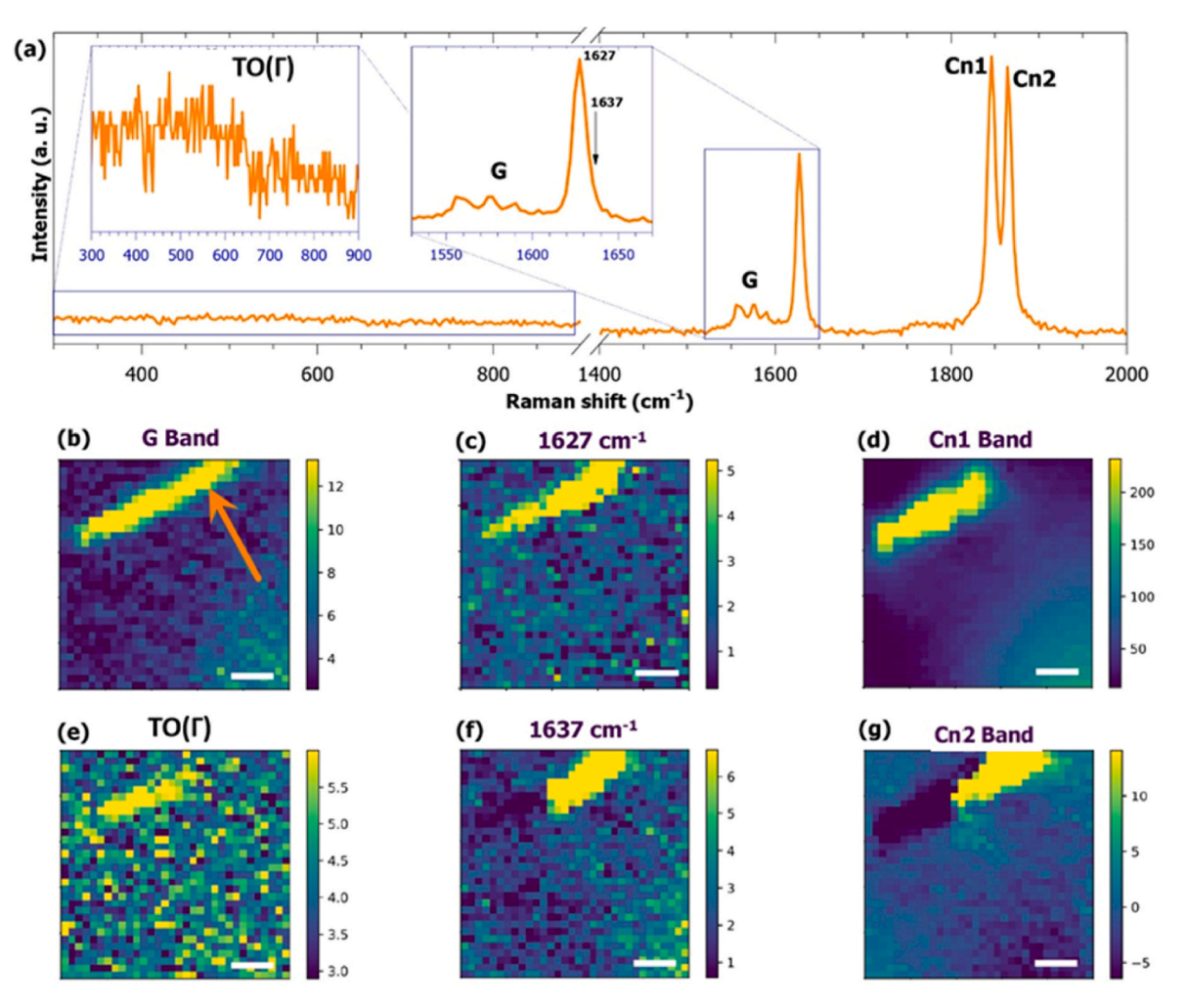


Fig. 4. (a) TERS spectrum obtained from an isolated LCC@MWCNT system at the position indicated by the orange arrow in (b); (b) Raman spectroscopic images of the carbon nanotube's G-band; (c) LA(X) mode at 1627 cm⁻¹ and (d) Cn mode at 1847 cm⁻¹; (e) TO(Γ) mode around 500 cm⁻¹; (f) LA(X) mode at 1637 cm⁻¹ and (g) Cn mode at 1866 cm⁻¹. The LA(X) Raman signatures can be correlated to different carbon chains by considering its spatial localization in the Raman mapping. The white scale bar is 50 nm. The spectral resolution is \pm 2 cm⁻¹.

frequency modes in multi-walled carbon nanotubes, although no phonon mode assignment was made [37]. The peak at 1637 cm⁻¹ (from now on LA(X) peak) could in principle be associated to the D′-band or other vibrational properties related only to the MWCNT but the Raman maps in Fig. 3e and f shows that this peak only occurs when the LCC Cn mode occurs. In the literature, this peak has been assigned as a signature for the bonding between LCCs with the hosting tubes when high pressure is applied [16]. We note, however, that in their case the vibrational properties of both LCC and hosting tubes are affected with an eventual disappearance of the Cn Raman mode. In our case, the measurements are performed under normal temperature and pressure, and the Cn mode is always present.

Additional TERS measurement was performed in a small LCC@MWCNT bundle. A typical Raman spectrum of such bundled system is shown in Fig. 4a, which is in very good agreement with the previous results. This spectrum was acquired in the position highlighted by the orange arrow in Fig. 4b. The Raman spectrum observed in Fig. 4a shows the G-band from the hosting MWCNTs together with a more intense and asymmetric peak that is deconvoluted into two bands each located at $1627~{\rm cm}^{-1}$ and $1637~{\rm cm}^{-1}$. We note that these frequencies are obtained from the fitting result using two distinct Lorentzian curves to fit such asymmetric feature (during the fitting process the amplitudes, centers and widths of the curves were free to vary). As discussed further in the text, these two peaks are associated with two distinct LCCs whose Cn modes resonate at $1847~{\rm cm}^{-1}$ (from now on Cn1, FWHM ~ 11.2

cm $^{-1}$) and 1866 cm $^{-1}$ (from now on Cn2, FWHM \sim 9.14 cm $^{-1}$). Both Cn1 and Cn2 are associated with individual chains of different lengths as supported by the symmetry of the peaks as well as their FWHM values. The G-band Raman map for the MWCNTs (Fig. 4b) reveals the spatial location of the entire carbon structure that constitutes the cluster. The TERS map in Fig. 4e shows that the LCC TO(Γ) around 500 cm $^{-1}$ is also present and matches the spatial location of the LCC's LA(X) and Cn bands.

The maps in Fig. 4c-d and Fig. 4f-g endorse that the Cn and LA(X) peaks are spatially correlated and come from specific LCCs. Fig. 4c maps the intensity of the Raman mode located at 1627 cm⁻¹, which correlates well with the peak at 1847 cm⁻¹ (Cn1 band) shown in Fig. 4d. Note that, although the 1627 cm⁻¹ peak intensity is not homogeneous, it extends throughout the whole spatial length observed for the Cn1 mode in Fig. 4d. We attribute the loss of contrast in the lower end of the LCC to an occasional misalignment between the tip apex and the laser hot spot center while raster-scanning. A similar analysis holds for the 1637 cm⁻¹ peak (Fig. 4f), which correlates well with the peak at 1866 cm⁻¹ (Cn2 band). It is also important to observe that, although the LA(X) and Cn spectroscopic images are also well spatially correlated with the $TO(\Gamma)$ peaks (Fig. 4e), the low intensity of such transverse signatures prevents their assignments to individual LCCs. It is also important to note that the presence of the LA(X) peak does not to affect the vibrational properties of the LCC Cn modes, and both modes coexist. These observations are in opposition to the aforementioned high-pressure (>13 GPa) experiments

[16], in which, due to an enhanced tube-chain cross-linking, a new peak (not found experimentally) was expected to appear around 1600 cm⁻¹ and the Cn mode disappears. It is important to rule out the assignment of the LA(X) peak to either the disorder induced D'-band [38] or to the periodic potential generated R-band [39,40], because if any of these assignments were correct, a correlation between the said D'-band (R-band) and the MWCNT D-band (extension length) should have been observed. Our data suggests that this novel LA(X) peak correlates only with the LCCs instead. Moreover, it is important to mention that both the D'- and R-bands reported in the literature are symmetric and much weaker than the G-band [41,42]. Except in Fig. 3, the LA(X) peaks shown in this work are asymmetric and as intense as (or much more intense in the case of TERS) than the G-band. These facts indicate that the LA(X), D' and R Raman modes have distinct natures.

We explain our assignments of the $\sim 1637 \text{ cm}^{-1}$ and 544 cm⁻¹ peaks to the LA(X) and $TO(\Gamma)$ modes, respectively, by comparison to state-ofthe-art first-principles calculations using density-functional theory (DFT). Initially, we compare our data to the calculated phonon dispersion shown in Fig. 2b of Romanin et al. [43]. Using hybrid exchange-correlation potentials and including quantum anharmonicity effects, they calculate vibrational frequencies of $\sim 1600 \text{ cm}^{-1}$ and $\sim 500 \text{ cm}^{-1}$ cm⁻¹ for the LA(X) and TO(Γ) modes, respectively, for the infinite chain. We reproduce and confirm these results by performing DFT calculations for both finite and infinite chains, using the hybrid and long-range corrected mCAM-B3LYP potential. Fig. 5 shows our calculated phonon density of states (DOS) for a finite chain of 120 carbon atoms. The figure also displays the atomic displacements for the various modes at the zone center (Γ) and zone edge (X). Frequencies are shifted with respect to experiments due to finite-size effects and because quantum anharmonicity effects - which generally produce frequency downshift [43] - are not included. Further details regarding our DFT calculations are found in the Supplementary Material (SM). In particular, we perform calculations for finite chains of different sizes and extrapolate the frequency values to the $N \to \infty$ limit, where *N* is the number of carbon atoms in the chain. Extrapolated values are $2173~\mathrm{cm}^{-1}$, $1564~\mathrm{cm}^{-1}$ and $657~\mathrm{cm}^{-1}$ for the LO (X), LA(X) and $TO(\Gamma)$ modes, respectively. We also performed calculations for the infinite chain (by applying periodic boundary conditions) yielding very similar results: 2195 cm⁻¹, 1590 cm⁻¹ and 678 cm⁻¹ respectively (see SM for further details). For comparison, the calculated LO(Γ) (or Cn) frequency is 1792 cm⁻¹ (extrapolated to $N \to \infty$).

Based on the comparison between theory and experiment, and by keeping in mind that we do not include quantum anharmonicity effects in the present calculations, we assign our measured Raman features at 1637 cm⁻¹ and 544 cm⁻¹ to the LA(X) and TO(Γ) modes, respectively. The $TO(\Gamma)$ mode corresponds to "zig-zag" displacements perpendicular to the chain axis, and it is a Raman-active mode for the infinite chain, in agreement with Casari et al. [35]. The LA(X) mode corresponds to vibrations in which the triple bond remains at rest and only the single bond is compressed/extended. Therefore, it probes directly the elasticity of the single bond in carbyne. As a zone-edge mode, it should not be Raman active for the infinite and perfect chain. We may speculate that it acquires a small Raman cross-section due to disorder effect. Interestingly, the LO(X) mode (theoretically at ~2180 cm⁻¹ according to our calculations), which is similar to the LA(X) mode but involves compression/extension of the triple bond only, is not observed in our Raman spectra. The reason for that is still elusive.

4. Conclusion

In this work, the linear carbon chain encapsulated by multi walled carbon nanotubes has been analyzed through far-field Raman microscopy and TERS. It was shown that the Raman spectrum profile of the bulk of the sample may be considered as a superposition of several spectra associated to individual LCC@MWCNT. It was also revealed by TERS that despite the high intensity peak (\sim 1800 cm $^{-1}$), there are others Raman actives modes related to the LCC@MWCNT at \sim 544 cm $^{-1}$

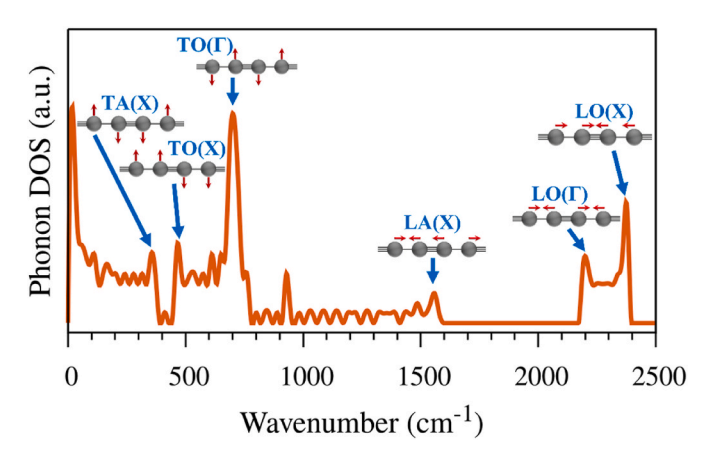


Fig. 5. Phonon density of states (DOS) of a finite LCC with 120 carbon atoms calculated via first-principles using density-functional theory (DFT). The DOS exhibits zone-center (Γ -point) and zone-edge (X-point) phonons. Our experiments report the observation of the, thus far elusive, $TO(\Gamma)$ and LA(X) modes. (A colour version of this figure can be viewed online.)

and $\sim 1637~{\rm cm}^{-1}$. The observation of such peaks was still elusive, and through our first-principles calculations, we determined that these frequencies are associated with the TO(Γ) and LA(X) modes of the LCC, respectively.

CRediT authorship contribution statement

Thiago A. Moura: Conceptualization, Methodology, Formal analvsis. Investigation. Writing – original draft. Writing – review & editing. Visualization. Wellington Q. Neves: Methodology, Formal analysis, Writing – original draft, Visualization. Rafael S. Alencar: Methodology, Formal analysis, Writing - original draft. Y.A. Kim: Resources. M. Endo: Resources. Thiago L. Vasconcelos: Resources, Methodology, Investigation, Resources, Writing - original draft. Deyse G. Costa: Formal analysis, Investigation, Writing - review & editing, Visualization. Graziâni Candiotto: Formal analysis, Investigation, Writing - review & editing, Visualization. Rodrigo B. Capaz: Methodology, Formal analysis, Investigation, Resources, Writing – review & editing, Visualization. Paulo T. Araujo: Methodology, Formal analysis, Investigation, Writing - original draft, Writing - review & editing, Visualization, Supervision, Project administration. Antonio G. Souza Filho: Conceptualization, Methodology, Writing - original draft, Writing - review & editing, Supervision, Project administration, Funding acquisition. Alexandre R. Paschoal: Conceptualization, Methodology, Formal analysis, Investigation, Resources, Writing - original draft, Writing - review & editing, Visualization, Supervision, Project administration, Funding acquisition.

Declaration of competing interest

The authors declare that they have no known competing financial interests or personal relationships that could have appeared to influence the work reported in this paper.

Acknowledgments

T.A.M. thanks Central Analítica/UFC for the support in confocal Raman analyses and the financial support from Brazilian agencies CNPq (168041/2017-0), CAPES and Funcap. A.R.P. thanks CNPq processes 426584/2016-3 and 314084/2021-5 and Funcap Pronex process PR2-011-00006.01-00/15 for the financial supports. P.T.A. is thankful to the National Science Foundation (NSF) under Grant No. [1848418] for the financial support. G.C. thanks FAPERJ, grant number E-26/200.627/2022 and E-26/210.391/2022 (project "Jovem Pesquisador Fluminense", process number 271814) for financial support and Núcleo

Avançado de Computação de Alto Desempenho (NACAD/COPPE/UFRJ), Sistema Nacional de Processamento de Alto Desempenho (SINAPAD) and Centro Nacional de Processamento de Alto Desempenho em São Paulo (CENAPAD-SP) for computational support.

Appendix A. Supplementary data

Supplementary data to this article can be found online at https://doi. org/10.1016/j.carbon.2023.118123.

References

- [1] W.A. Chalifoux, R.R. Tykwinski, Synthesis of polyynes to model the sp-carbon allotrope carbyne, Nat. Chem. 2 (2010) 967–971, https://doi.org/10.1038/ nchem.828.
- [2] F. Cataldo, Stability of polyynes in air and their degradation by ozonolysis, 91, https://doi.org/10.1016/j.polymdegradstab.2005.04.046, 2006.
- [3] M. Kertesz, S. Yang, Energetics of linear carbon chains in one-dimensional restricted environment, Phys. Chem. Chem. Phys. 11 (2009) 425–430, https://doi. org/10.1039/b812635f.
- [4] S. Toma, M. Irita, Bulk synthesis of linear carbon chains confined inside single-wall carbon nanotubes by vacuum discharge, 131–135, https://doi.org/10.1002/sia.6590, 2019.
- [5] C. Zhao, R. Kitaura, H. Hara, S. Irle, H. Shinohara, Growth of linear carbon chains inside thin double-wall carbon nanotubes, J. Phys. Chem. C 115 (2011) 13166–13170, https://doi.org/10.1021/jp201647m.
- [6] X. Zhao, Y. Ando, Y. Liu, M. Jinno, T. Suzuki, Carbon nanowire made of a long linear carbon chain inserted inside a multiwalled carbon nanotube, Phys. Rev. Lett. 90 (2003), 187401, https://doi.org/10.1103/PhysRevLett.90.187401.
- [7] L. Shi, P. Rohringer, K. Suenaga, Y. Niimi, J. Kotakoski, J.C. Meyer, H. Peterlik, M. Wanko, S. Cahangirov, A. Rubio, Z.J. Lapin, L. Novotny, P. Ayala, T. Pichler, Confined linear carbon chains as a route to bulk carbyne, Nat. Mater. 15 (2016) 634–639, https://doi.org/10.1038/nmat4617.
- [8] D. Nishide, H. Dohi, T. Wakabayashi, E. Nishibori, S. Aoyagi, M. Ishida, S. Kikuchi, R. Kitaura, T. Sugai, M. Sakata, H. Shinohara, Single-wall carbon nanotubes encaging linear chain C10H2 polyyne molecules inside, Chem. Phys. Lett. 428 (2006) 356–360, https://doi.org/10.1016/j.cplett.2006.07.016.
- [9] S. Iijima, Helical microtubules of graphitic carbon, Nature (1991) 56-58.
- [10] R.F. C, R.E.S.H.W. Kroto, J.R. Heath, S.C. O'Brien, C60: buckminsterfullerene, Nature 318 (1985) 162–163.
- [11] J.M. Raimond, M. Brune, Q. Computation, F. De Martini, C. Monroe, Electric field effect in atomically, Thin Carbon Films 306 (2004) 666–670.
- [12] S. Kotrechko, I. Mikhailovskij, T. Mazilova, E. Sadanov, A. Timoshevskii, N. Stetsenko, Y. Matviychuk, Mechanical properties of carbyne: experiment and simulations, Nanoscale Res. Lett. 10 (2015) 2–7, https://doi.org/10.1186/s11671-015-0761-2.
- [13] O. Cretu, I. Janowska, Electrical Conductivity Measured in Atomic Carbon Chains, Arxiv Prepr., 2013, pp. 1–21.
- [14] M. Liu, V.I. Artyukhov, H. Lee, F. Xu, B.I. Yakobson, Carbyne from first principles: chain of c atoms, a nanorod or a nanorope, ACS Nano 7 (2013) 10075–10082, https://doi.org/10.1021/nn404177r.
- [15] W.Q. Neves, R.S. Alencar, R.S. Ferreira, A.C. Torres-Dias, N.F. Andrade, A. San-Miguel, Y.A. Kim, M. Endo, D.W. Kim, H. Muramatsu, A.L. Aguiar, A.G. Souza Filho, Effects of pressure on the structural and electronic properties of linear carbon chains encapsulated in double wall carbon nanotubes, Carbon N. Y. 133 (2018) 446–456, https://doi.org/10.1016/j.carbon.2018.01.084.
- [16] W.Q. Neves, R.S. Ferreira, Y.A. Kim, M. Endo, G.B. Choi, H. Muramatsu, A. L. Aguiar, R.S. Alencar, A.G.S. Filho, Pressure-induced structural transformations on linear carbon chains encapsulated in carbon nanotubes: a potential route for obtaining longer chains and ultra-hard composites, Carbon N. Y. 196 (2022) 20–28. https://doi.org/10.1016/j.carbon.2022.03.045.
- [17] M.S. Dresselhaus, G. Dresselhaus, R. Saito, A. Jorio, Raman spectroscopy of carbon nanotubes, Phys. Rep. 409 (2005) 47–99, https://doi.org/10.1016/j. physrep.2004.10.006.
- [18] L. Shi, P. Rohringer, M. Wanko, A. Rubio, S. Waßerroth, S. Reich, S. Cambré, W. Wenseleers, P. Ayala, T. Pichler, Electronic band gaps of confined linear carbon chains ranging from polyyne to carbine, Phys. Rev. Materials 1 (2017), 075601, https://doi.org/10.1103/PhysRevMaterials.1.075601.
- [19] J. Wu, H. Xu, J. Zhang, Raman spectroscopy of graphene, Hua Hsueh Hsueh Pao (2014) 301–318, https://doi.org/10.6023/A13090936.
- [20] S. Heeg, L. Shi, T. Pichler, L. Novotny, Raman resonance profile of an individual confined long linear carbon chain, Carbon N. Y. 139 (2018) 581–585, https://doi. org/10.1016/j.carbon.2018.07.007.
- [21] C.D. Tschannen, G. Gordeev, S. Reich, L. Shi, T. Pichler, M. Frimmer, L. Novotny, S. Heeg, Raman scattering cross section of confined carbyne, Nano Lett. 20 (2020) 6750–6755, https://doi.org/10.1021/acs.nanolett.0c02632.
- [22] N.L. Costa, K. Sharma, Y.A. Kim, G.B. Choi, M. Endo, N.M. Barbosa Neto, A. R. Paschoal, P.T. Araujo, Thermodynamics of linear carbon chains, Phys. Rev. Lett. 126 (2021), 125901, https://doi.org/10.1103/PhysRevLett.126.125901.

- [23] K. Sharma, N.L. Costa, Y.A. Kim, H. Muramatsu, N.M. Barbosa Neto, L.G.P. Martins, J. Kong, A.R. Paschoal, P.T. Araujo, Anharmonicity and universal response of linear carbon chain mechanical properties under hydrostatic pressure, Phys. Rev. Lett. 125 (2020), 105501, https://doi.org/10.1103/PhysRevLett.125.105501.
- [24] Y.A. Kim, H. Muramatsu, T. Hayashi, M. Endo, Catalytic metal-free formation of multi-walled carbon nanotubes in atmospheric arc discharge, Carbon N. Y. 50 (2012) 4588–4595, https://doi.org/10.1016/j.carbon.2012.05.044.
- [25] N.F. Andrade, T.L. Vasconcelos, C.P. Gouvea, B.S. Archanjo, C.A. Achete, Y.A. Kim, M. Endo, C. Fantini, M.S. Dresselhaus, A.G. Souza Filho, Linear carbon chains encapsulated in multiwall carbon nanotubes: resonance Raman spectroscopy and transmission electron microscopy studies, Carbon N. Y. 90 (2015) 172–180, https://doi.org/10.1016/j.carbon.2015.04.001.
- [26] N.F. Andrade, A.L. Aguiar, Y.A. Kim, M. Endo, P.T.C. Freire, G. Brunetto, D. S. Galvão, M.S. Dresselhaus, A.G. Souza Filho, Linear carbon chains under high-pressure conditions, J. Phys. Chem. C 119 (2015) 10669–10676, https://doi.org/10.1021/acs.jpcc.5b00902.
- [27] W.Q. Neves, R.S. Ferreira, Y.A. Kim, M. Endo, G.B. Choi, H. Muramatsu, A. L. Aguiar, R.S. Alencar, A.G. Souza Filho, Pressure-induced structural transformations on linear carbon chains encapsulated in carbon nanotubes: a potential route for obtaining longer chains and ultra-hard composites, Carbon N. Y. 196 (2022) 20–28, https://doi.org/10.1016/j.carbon.2022.03.045.
- [28] T.L. Vasconcelos, B.S. Archanjo, B.S. Oliveira, R. Valaski, R.C. Cordeiro, H. G. Medeiros, C. Rabelo, A. Ribeiro, P. Ercius, C.A. Achete, A. Jorio, L.G. Cançado, Plasmon-tunable tip pyramids: monopole nanoantennas for near-field scanning optical microscopy, Adv. Opt. Mater. 6 (2018) 1–6, https://doi.org/10.1002/adom.201800528.
- [29] S. Heeg, L. Shi, L.V. Poulikakos, T. Pichler, L. Novotny, Carbon nanotube chirality determines properties of encapsulated linear carbon chain, Nano Lett. 18 (2018) 5426–5431, https://doi.org/10.1021/acs.nanolett.8b01681.
- [30] M. Martinati, W. Wenseleers, L. Shi, S. Md Pratik, P. Rohringer, W. Cui, T. Pichler, V. Coropeanu, Jean-Luc Brédas, S. Cambré, Electronic structure of confined carbyne from joint wavelength-dependent resonant Raman spectroscopy and density functional theory investigations, Carbon 189 (2022) 276–283, https://doi. org/10.1016/j.carbon.2021.12.059.
- [31] R. Kato, S. Igarashi, T. Umakoshi, P. Verma, Tip-enhanced Raman spectroscopy of multiwalled carbon nanotubes through D-band imaging: implications for nanoscale analysis of interwall interactions, ACS Appl. Nano Mater. 3 (2020) 6001–6008, https://doi.org/10.1021/acsanm.0c01188.
- [32] E.A. Buntov, A.F. Zatsepin, M.B. Guseva, Y.S. Ponosov, 2D-ordered kinked carbyne chains: DFT modeling and Raman characterization, Carbon N. Y. 117 (2017) 271–278, https://doi.org/10.1016/j.carbon.2017.03.010.
- [33] C.D. Tschannen, T.L. Vasconcelos, L. Novotny, Tip-enhanced Raman spectroscopy of confined carbon chains, J. Chem. Phys. 156 (2022), https://doi.org/10.1063/ 5.0073050
- [34] C.S. Casari, M. Tommasini, R.R. Tykwinski, A. Milani, Carbon-atom wires: 1-D systems with tunable properties, Nanoscale 8 (2016) 4414–4435, https://doi.org/ 10.1039/c5pr06175i.
- [35] C.S. Casari, A. Li Bassi, A. Baserga, L. Ravagnan, P. Piseri, C. Lenardi, M. Tommasini, A. Milani, D. Fazzi, C.E. Bottani, P. Milani, Low-frequency modes in the Raman spectrum of sp-s p2 nanostructured carbon, Phys. Rev. B Condens. Matter 77 (2008) 1–7, https://doi.org/10.1103/PhysRevB.77.195444.
- [36] F. Liu, X. Tang, W. Du, B. Chi, X. Zhao, Y. Liu, Radial and axial vibration modes of graphyne nanotubes, Mater. Today Commun. 31 (2022), 103610, https://doi.org/ 10.1016/j.mtcomm.2022.103610.
- [37] M. Jinno, S. Bandow, Y. Ando, Multiwalled carbon nanotubes produced by direct current arc discharge in hydrogen gas, Chem. Phys. Lett. 398 (2004) 256–259, https://doi.org/10.1016/j.cplett.2004.09.064.
- [38] R. Tsu, H.J. González, I. Hernández C, Observation of splitting of the E2g mode and two-phonon spectrum in graphites, Solid State Commun. 27 (1978) 507–510, https://doi.org/10.1016/0038-1098(78)90382-4.
- [39] V. Carozo, C.M. Almeida, E.H.M. Ferreira, L.G. Cançado, C.A. Achete, A. Jorio, Raman signature of graphene superlattices, Nano Lett. 11 (2011) 4527–4534, https://doi.org/10.1021/nl201370m.
- [40] V. Carozo, C.M. Almeida, B. Fragneaud, P.M. Bedê, M.V.O. Moutinho, J. Ribeiro-Soares, N.F. Andrade, A.G. Souza Filho, M.J.S. Matos, B. Wang, M. Terrones, R. B. Capaz, A. Jorio, C.A. Achete, L.G. Cançado, Resonance effects on the Raman spectra of graphene superlattices, Phys. Rev. B Condens. Matter 88 (2013) 1–10, https://doi.org/10.1103/PhysRevB.88.085401.
- [41] M.S. Dresselhaus, A. Jorio, A.G. Souza Filho, R. Saito, Defect characterization in graphene and carbon nanotubes using Raman spectroscopy, Philos. Trans. R. Soc. A Math. Phys. Eng. Sci. 368 (2010) 5355–5377, https://doi.org/10.1098/ rsta.2010.0213.
- [42] M.A. Pimenta, G. Dresselhaus, M.S. Dresselhaus, L.G. Cançado, A. Jorio, R. Saito, Studying disorder in graphite-based systems by Raman spectroscopy, Phys. Chem. Chem. Phys. 9 (2007) 1276–1291, https://doi.org/10.1039/b613962k.
- [43] D. Romanin, L. Monacelli, R. Bianco, I. Errea, F. Mauri, M. Calandra, Dominant role of quantum anharmonicity in the stability and optical properties of infinite linear acetylenic carbon chains, J. Phys. Chem. Lett. 12 (2021) 10339–10345, https:// doi.org/10.1021/acs.jpclett.1c02964.